



Deposited via The University of Leeds.

White Rose Research Online URL for this paper:

<https://eprints.whiterose.ac.uk/id/eprint/93040/>

Version: Accepted Version

Article:

Vukovic, N, Danicic, A, Radovanovic, J et al. (2015) Possibilities of achieving negative refraction in QCL-based semiconductor metamaterials in the THz spectral range. *Optical and Quantum Electronics*, 47 (4). 883 - 891. ISSN: 0306-8919

<https://doi.org/10.1007/s11082-014-0020-2>

Reuse

Items deposited in White Rose Research Online are protected by copyright, with all rights reserved unless indicated otherwise. They may be downloaded and/or printed for private study, or other acts as permitted by national copyright laws. The publisher or other rights holders may allow further reproduction and re-use of the full text version. This is indicated by the licence information on the White Rose Research Online record for the item.

Takedown

If you consider content in White Rose Research Online to be in breach of UK law, please notify us by emailing eprints@whiterose.ac.uk including the URL of the record and the reason for the withdrawal request.

Possibilities of achieving negative refraction in QCL-based semiconductor metamaterials in the THz spectral range

Nikola Vuković¹, Aleksandar Daničić²,
Jelena Radovanović¹, Vitomir Milanović¹ and Dragan Indjin³

¹*School of Electrical Engineering, University of Belgrade, Bulevar Kralja Aleksandra 73, 11000 Belgrade, Serbia*

²*P* group, Vinca Institute of Nuclear Sciences, University of Belgrade - P.O.B.522,11001 Belgrade, Serbia*

³*School of Electronic and Electrical Engineering, University of Leeds, Leeds LS2 9JT, UK*

Abstract: One of the challenges in the design of metamaterials' unit cells is the reduction of losses caused by the metallic inclusions. In order to overcome this obstacle, it has been proposed to use the active medium as the unit cell. Quantum cascade lasers are great candidates for the active medium materials since they are able to provide high values of optical gain. In this paper we investigate and compare two quantum cascade structures optimized for emission frequencies lower than 2 THz and simulate the effect of a strong magnetic field applied perpendicularly to the layers. Comprehensive description of conduction-band nonparabolicity is used to calculate the electronic structure, and subsequently evaluate the longitudinal optical phonon and interface roughness scattering rates and solve the system of rate equations which govern the distribution of carriers among the Landau levels. Once we assess the degree of population inversion, we have all the necessary information about the permittivity component along the growth direction of the structure and may determine the conditions under which the structure displays negative refraction.

Keywords: Semiconductor Metamaterials, Quantum Cascade Laser, Magnetic field, negative refraction

Introduction

New artificially assembled effective media, electromagnetic composites named metamaterials (MTMs), with a predominant feature of exhibiting properties otherwise not found in nature, such as optical magnetism and negative refraction, have been investigated in recent years [1-4]. Metamaterials are comprised of composite elements patterned in periodic arrays, significantly smaller than the wavelength of interest so that the wave propagation occurs according to refraction through the effective medium, instead of diffraction, as it is the case of photonic crystals [5].

Negative refractive index media were first demonstrated at microwave frequencies [6], followed by a demonstration of functional metamaterials at near-infrared and visible frequencies [7, 3]. Most of the left-handed metamaterials are based on metal inclusions, which introduce high losses at frequencies of interest and therefore limit the applicability [8, 9]. Although the metal split-ring resonators have been the most common design for THz two-dimensional planar metamaterials, some alternative composite right/left-handed metamaterial (CRLH) waveguide designs have been proposed [10] as well.

A metamaterial where metallic inclusion are replaced with semiconductor based low-dimensional quantum structures exhibits significantly lower losses in the infrared, as these nanostructures are a source of gain [10]. The THz frequency range is well suited for exploration of such phenomena, since quantum cascaded structures with subwavelength dimensions can be readily obtained using modern fabrication techniques, and optical gain is available through intersubband transitions in THz quantum cascade laser (QCL) [11].

THz QCLs are the longest wavelength semiconductor laser sources, covering the spectral range from 0.6-5THz [12]. After their first demonstration, QCLs have become the preferred compact sources in THz region, even though the integration of a THz source and detector is still challenging. Nevertheless, they are essential for applications in THz imaging and sensing, while their ability to operate in continuous wave regime makes them suitable for high

· Corresponding author Tel.: +381113370088
e-mail adress: radovanovic@etf.bg.ac.rs

resolution THz spectroscopy [13, 14]. Metal-metal THz QCL waveguides are the most suitable platform for active THz CRLM metamaterial implementation [4].

In this paper, we analyze the realization of metamaterials based on quantum cascaded structures which are able to deliver high-enough values of the optical gain to achieve negative refraction within a range of frequencies. The layers configuration corresponds to the quantum cascade laser and the structures are subjected to a strong magnetic field, used to manipulate the carrier scattering processes by discretizing the in-plane electron motion, finally affecting the optical gain [15] and the relevant component of dielectric permittivity.

2. Theoretical consideration

Quantum cascade laser is a low-dimensional semiconductor quantum structure that consists of series of identical stages. As electron travels through the structure, it emits a number of photons which is (in an ideal scenario) equal to the number of periods. The devices are thus designed to include electronic subbands defined as the upper and the lower laser state, electric pumping along the growth direction, as well as periodic repetition of active elements responsible for the light amplification. Dynamic properties of QCLs differ from those of interband lasers, as very fast non-radiative intersubband scattering mechanisms take place on a timescale of several picoseconds [16]. Although being limited by operating temperature problems, which are still below the level reachable with Peltier cooling elements, THz QCLs are nevertheless in the focus of research attention, and recent developments have led to significantly simplified active region designs [17]. The number of wells per period has been reduced, starting from the superlattice-based structure that comprised 7 wells (in the first demonstration) [12], down to two-well diagonal design [17]. The influence of external magnetic field on QCL's output properties is of special interest. A lot of research has been put in investigating different scattering mechanisms in the magnetic field assisted structures, as it may improve the QCL performance at longer wavelengths [15]. In our modeling of QCLs we take particular care to implement the meticulous description of conduction-band (CB) nonparabolicity effects (NPE). Our method of choice for description of NPE originates from [18] where the author used bulk CB dispersion expanded up to the fourth order in wave vector. He used parameters from a 14-band k.p model which assumes interaction of the lowest CB with the light-hole band, split-off band and higher CBs, presented in [19].

The Schrödinger equation for the envelope wave function $\eta_n(z)$ of a heterostructure placed in the electric field of strength K reads:

$$\frac{d^2}{dz^2} \alpha_0(z) \frac{d^2 \eta_n(z)}{dz^2} - \frac{\hbar^2}{2} \frac{d}{dz} \frac{1}{m^*(z)} \frac{d\eta_n(z)}{dz} + (U(z) - eKz) \eta_n(z) = \varepsilon_n \eta_n(z), \quad (1)$$

where m^* is the effective mass at the bottom of the conduction-band, e is the electron charge, ε_n is the confinement energy at the bottom of the n -th subband and \mapsto_0 is the nonparabolicity parameter from [19]. If the concentration of ionized impurities is not extensive, we may adopt that the potential energy $U(z)$ originates from the conduction-band discontinuity only. The two boundary conditions at the interface of two semiconductors are described in detail in [20]. The second boundary condition is derived by double integration of the Schrödinger equation and imposes the conservation of probability current. The formula (1) is valid at the bottom of energy subbands where the in-plane wave vector k_{\parallel} equals zero, otherwise it should include additional terms proportional to x and y components of k_{\parallel} .

In the absence of external magnetic field B , the energy dispersion relation of the n -th subband is $\varepsilon_n + \hbar^2 k_{\parallel}^2 / (2m_{\parallel n})$, where the in-plane mass of is calculated as:

$$\frac{1}{m_{\parallel n}} = \int \eta_n^* \frac{1}{m^*(z)} \eta_n dz - \frac{2}{\hbar^2} \int \eta_n^* \frac{d}{dz} (2\alpha_0 + \beta_0) \frac{d\eta_n}{dz} dz. \quad (2)$$

When the perpendicular magnetic field of strength B is applied, continuous 2D subbands transform into discrete Landau levels (LLs) with indices l , according to the formula:

$$E_{n,l} = \varepsilon_n + (l + \frac{1}{2}) \frac{\hbar e B}{2} + \frac{e^2 B^2}{2\hbar^2} \left[(8l^2 + 8l + 5) \langle \alpha_0 \rangle_n + (l^2 + l + 1) \langle \beta_0 \rangle_n \right]. \quad (3)$$

Here $\langle \alpha_0 \rangle_n$ and $\langle \beta_0 \rangle_n$ are nonparabolicity parameters from [18] averaged along the z axes. It can be shown that the optical transitions are possible only between the LLs with the same value of index l . Magnetic field clearly affects the energy spectrum, thus it can be used as a tool to purposely modify scattering rates between levels of interest, and therefore affect the optical gain, as described in [15].

Electron energy levels in magnetic field are given by Eq. (3), which is obtained from the perturbation theory. As for the wavefunctions, we assume that they are independent of magnetic field, and equal to wavefunction for zero-field case, which implies that the dipole matrix elements are taken as independent of magnetic field as well. Similar approximation is used in analysis of electronic structure of QCL (in the absence of magnetic field), when the transition matrix element is assumed to be independent of the in-plane wavevector. By using the time-independent perturbation theory (as in the case of deriving Eq. (3)), an analytic expression for the dependence of the matrix element on B can be derived. We will give here our initial, merely numerical results for the change in the matrix elements with magnetic field. For $B = 10\text{T}$, and taking into account the lowest transition corresponding to the Landau index $l = 0$, the matrix element is reduced by 3.5% due to the influence of magnetic field. Evidently, the changes will be higher for stonger magnetic fields and higher values of the Landau index. The derivation of the analytic expression for the change of transition matrix element with magnetic field, will be the subject of our future work, soon to be published.

As most of the proposed and so far demonstrated metamaterial structures include some form of metallic layers (metallic films, wires, spheres, etc.), it is expected for those structures to exhibit very high optical losses, which could turn out to be detrimental to their performance [18,19]. As pointed out above, it is very important to compensate the losses by using active metamaterials with high values of optical gain. Therefore, a QCL-like structure may be a good solution since it offers the possibility to generate substantial optical gain via carrier injection at specific frequencies [20].

For quantum well based semiconductor nanostructures with strong anisotropy of optical properties the dielectric permittivity tensor has the form [6]:

$$\|\varepsilon\| = \begin{vmatrix} \varepsilon_{\parallel} & 0 & 0 \\ 0 & \varepsilon_b & 0 \\ 0 & 0 & \varepsilon_{\perp} \end{vmatrix}, \quad (4)$$

while the relative magnetic permeability $\mu = 1$. Here, ε_{\parallel} is the permittivity component along the quantum well planes, and equals ε_b -the average permittivity of the background material. Permittivity along growth axes (z) is denoted by ε_{\perp} and can be described by Lorentzian model [21]:

$$\varepsilon_{\perp} = \varepsilon_b + \frac{e^2}{\varepsilon_0 L h} \sum_{f \leftarrow i} (N_{S,f} - N_{S,i}) \frac{|d_{f,i}|^2}{(\omega_{i,f} - \omega) - i\gamma_{i,f}} \quad (5)$$

where L is the unit cell length in z -direction, $N_{S,j}$ represents the electron sheet density in j th state, $\omega_{i,f}$ is the resonant transition frequency between the initial and the final state (i and f , respectively), ω is the frequency of the input light, $\gamma_{i,f}$ stands for the transition linewidth, while $d_{f,i}$ denotes the transition matrix element between the final and initial state. As it may be concluded from the above equation, the normal component of dielectric permittivity strongly depends on electron sheet density in the states of interest. The criteria for achieving the negative refraction in the case of anisotropic single-negative MTM read [22]:

$$\varepsilon_{\parallel} > 0, \quad \text{Re}(\varepsilon_{\perp}) < 0 \quad (6)$$

It is clear from Eq. (5) that in order to obtain the negative values of the real part of ε_{\perp} , one has to achieve high population inversion ($N_{S,f} - N_{S,i}$). To manage that, it is essential to provide fast depopulation of the lower laser state. The main mechanism responsible for depopulation is the electron-longitudinal optical (LO) phonon scattering. Unlike QCLs operating in the mid-infrared range, where electron-acoustic (AC) phonon scattering may have an important contribution to the total relaxation rate, when it comes to THz QCLs this scattering mechanism is found to be negligible. Instead, interface roughness scattering (IRS) must be included since there is a significant overlap between the wave functions of the adjacent periods. The total scattering rate of the system can be defined as:

$$W_{E_i \rightarrow E_f} = W_{E_i \rightarrow E_f}^{LO} + \sum_{z_i} W_{E_i \rightarrow E_f}^{IRS} \quad (7)$$

where $W_{E_i \rightarrow E_f}^{LO}$ denotes the LO phonon scattering rate between the initial and the final state, while $W_{E_i \rightarrow E_f}^{IRS}$ is the interfaces roughness scattering rate, calculated at every surface z_i .

In order to evaluate the dielectric permittivity we need to determine the electron distribution over all LLs by solving the full system of rate equations:

$$\frac{\partial N_f}{\partial t} = \bar{f}_f \sum_{i \neq f} N_i W_{E_i \rightarrow E_f} - N_f \sum_{i \neq f} \bar{f}_i W_{E_f \rightarrow E_i} = 0 \quad (8)$$

Here i, f define the initial and the final state, and run through all the Landau levels, with all periods included, while $\bar{f}_i = 1 - \pi \hbar / (eB) N_i$ relates to the probability of state i being unoccupied [23]. As QCL consists of repetitive elements (periods), the system of rate equations can be simplified as described in [24]. We assume that inside the cascade there is a globally linear potential variation, which enables the use of periodic boundary conditions for the surface densities. For each period we select the identical set of N Landau levels, with the same electron distribution. When solving the system of rate equations, there are $N - 1$ linearly independent equations, and the remaining one is replaced by the particle conservation law, which reads: $\sum_i N_i = N_s$, with N_s being the total electron sheet density.

As evident from Eq. (8), we have used in this work the method of empirical rate equations, which is considered as a starting method in QCL analysis, since it accounts for the electron density of subbands only. The analysis of non-equilibrium distribution within subbands is enabled by the Monte Carlo method [26]. Quantum mechanical generalization of the empirical rate equations method is one-dimensional density matrix method, which includes the effects of resonant tunneling and dephasing [26]. On the other hand, three-dimensional density matrix method may be viewed as a generalization of the method based on the Boltzmann equation and takes into account the consideration of the in-plane wave vector [26]. It is well known that the non-equilibrium Green's function (NEGF) theory [27-30] represents the most sophisticated and the most general method for the description of coherent and non-coherent transport; however, this method requires the most memory and CPU time in numerical simulations. All the methods listed above, apart from the empirical rate equations method, in particular the NEGF theory, would yield more precise results in both qualitative and quantitative sense, and will be considered in our future work.

3. Numerical results

We investigate two QCL active region designs, with three and four quantum wells per period, biased by external electric field. Both structures belong to the THz part of the spectrum, lasing at 1.45 THz and 1.9 THz, as described in [14] and [25] respectively. The active region is surrounded by the collector/emitter barriers, which enable carrier injection from the preceding active region/extraction from the lower subband to the next region [14]. Both analyzed structures are realized in GaAs/Al_{0.15}Ga_{0.85}As and have small design bias of approximately 9 kVcm⁻¹.

Fig.1a. shows the three-level intrawell-phonon QCL designed for 1.45 THz emission which has radiative transition between levels 3 and 2, while fast electron-LO phonon scattering depopulates laser subband 2 to level 1. The level 4 is an additional upper subband which we included in calculations in perpendicular magnetic field for reasons of accuracy. Fig.1b. shows the four level scheme in which each level participates in the transportation process. At resonance, electrons are injected into the upper level 4 from the injector level 1 of the preceding period. Radiative transition occurs between levels 4 and 3, after which the electrons are extracted from lower level 3 (which is in resonance with level 2) by LO phonon scattering into level 1.

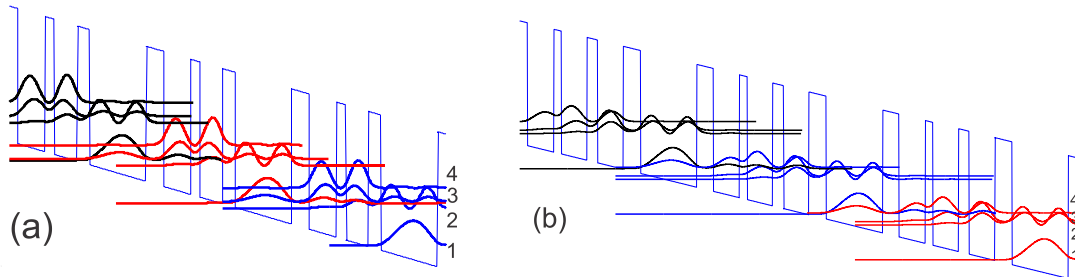


Fig. 1. Conduction band profiles consisting of three periods (modules) in case of: (a) three-well module lasing at 1.45 THz, and (b) four-well module lasing at 1.9 THz.

These structural designs utilize the diagonal transitions and thus have longer upper laser state lifetime and provide larger population inversion. The latter is especially important at high operating temperatures, when LO-phonons are thermally activated and affect the population inversion [12]. The expressions for evaluating the relevant relaxation rates of these structures are described in detail in [15], where we observed electron-LO phonon scattering and interface roughness scattering. The temperature is kept constant in both cases and amounts to 77K. After summing up the contributions of both interface roughness scattering and electron-LO phonon scattering, as defined by Eq.(7), we calculate the total scattering rate. Using Eq. (8) we solve the full system of rate equations, while the modal gain is calculated as in [15], and here is presented in Fig (2).

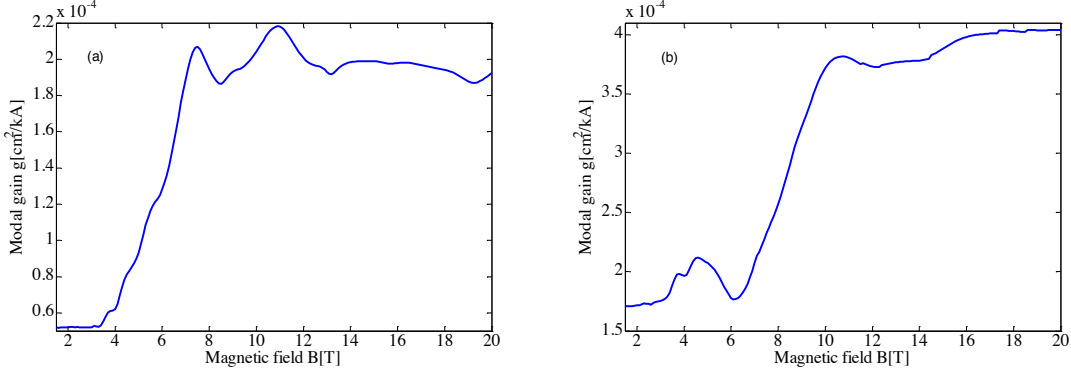


Fig. 2. Modal gain as a function of the applied magnetic field: (a) three-well structure designed for 1.45 THz emission, and (b) four-well structure designed for 1.9 THz. Gain is calculated for total carrier sheet density of $2.2 \times 10^{14} \text{ m}^{-2}$.

Following Eq. (5), one can calculate the values of $\epsilon_{\perp} = \epsilon_R + i\epsilon_I$. For some values of magnetic field and total carrier sheet density N_s it is possible to achieve negative values of ϵ_R , the real part of ϵ_{\perp} , Fig(3a). Thus, for a given structure we expect to get lower negative values of ϵ_R at positions with higher gain. On the other hand, if the sheet density N_s is large enough, negative ϵ_R is reached even for lower values of magnetic field B , as long as the population inversion is maintained, as depicted in Fig(3b). From Fig(3b) we can see that in case of both structures, for $N_s=7 \times 10^{16} \text{ m}^{-2}$, we can find negative value of ϵ_R for all magnitudes of B between 1.5 T and 20 T. Note that profiles of minimum values of ϵ_R look like inverted modal gain profiles from Fig(2), which we anticipated, since both gain and ϵ_R are proportional to the inverse population but with a different sign. From Fig(3b) we also see that for B between 5.5 T and 9.1 T 3-well design achieves lower ϵ_R , while for other values of B , 4-well design happens to be a better choice for negative ϵ_R .

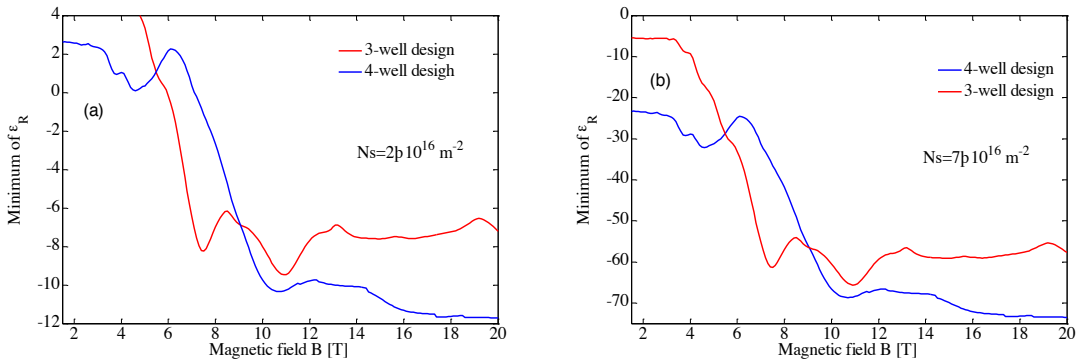


Fig. 3. The dependence of the minimum value of ϵ_R on magnetic field B for both structures: (a) for $N_s=2 \times 10^{16} \text{ m}^{-2}$ and (b) $N_s=7 \times 10^{16} \text{ m}^{-2}$.

Fig.(4) illustrates the dependence of the real and imaginary parts of ϵ_{\perp} on frequency, and the results are presented for different values of magnetic field B. The real and imaginary parts of ϵ_{\perp} are denoted by full lines and dashed lines respectively, for N_s of $7 \times 10^{16} \text{ m}^{-2}$. For the same values of N_s and similar value of B (approximately 11 T) 4-well design has slightly lower minimum values of ϵ_R and broader range of frequencies where ϵ_R has negative values. For example, for $N_s=10^{17} \text{ m}^{-2}$ structure from Fig(1a) has $\epsilon_R = -99.34$ (at $\omega=7.2$ THz), while the structure from Fig(1b) has $\epsilon_R = -103.7$ (at $\omega=10.5$ THz). Maximum value of ω for which the 3-well design has negative ϵ_R is 10 THz while the critical value for the 4-well design is 13.3 THz.

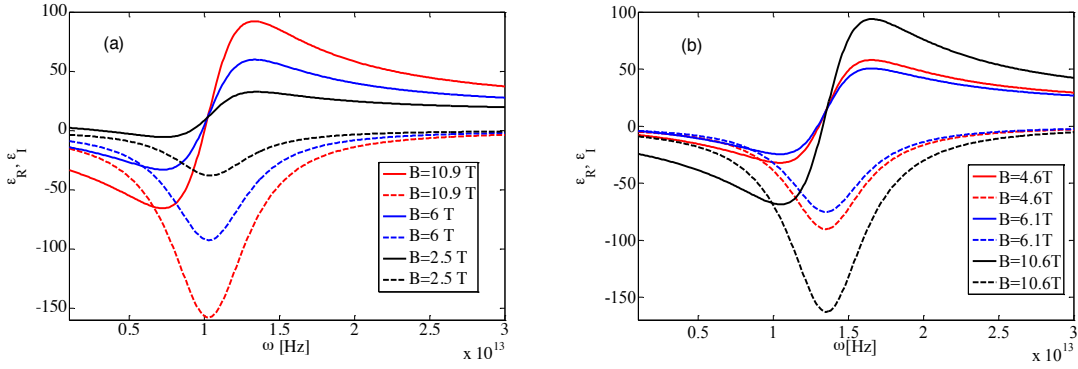


Fig. 4. The dependence of the real part of ϵ_{\perp} (ϵ_R , full lines) and the imaginary part (ϵ_I , dashed lines) on frequency for various values of magnetic field B: (a) three-well structure lasing at 1.45 THz, and (b) four-well structure lasing at 1.9 THz. In these calculations total carrier sheet density N_s is $7 \times 10^{16} \text{ m}^{-2}$.

Another set of calculations is done to determine the critical values of the total sheet density for which we achieve negative refraction. From Fig(3) we can find the magnitudes of B for which ϵ_R has the lowest value. We changed the N_s between 10^{16} m^{-2} and 10^{17} m^{-2} for both QCL structures, and plotted the results in Fig.(5). Both in 3-well and 4-well design, minimal N_s is determined to be $2 \times 10^{16} \text{ m}^{-2}$.

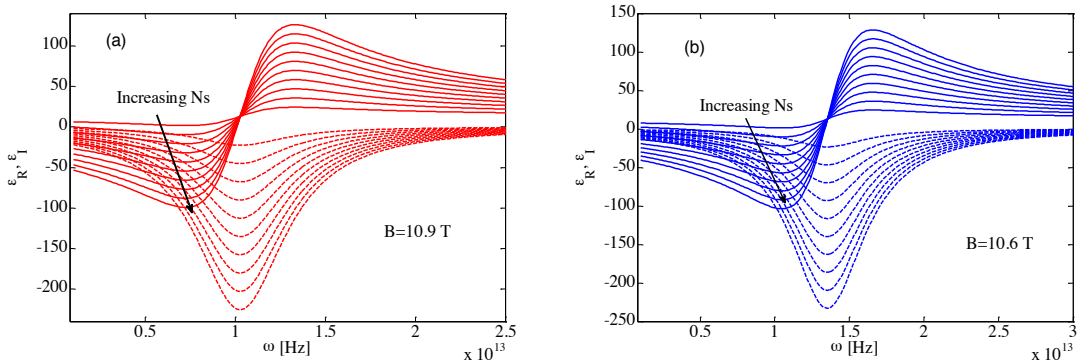


Fig. 5. The dependence of real part of ϵ_{\perp} (ϵ_R , full lines) and the imaginary part (ϵ_I , dashed lines) on frequency for various values of total carrier sheet density N_s in case of: (a) three-well structure lasing at 1.45 THz, and (b) four-well structure lasing at 1.9 THz. N_s is varied from 10^{16} m^{-2} to 10^{17} m^{-2} with 10^{16} step.

4. Conclusion

We show that the structures fabricated and described in [14, 25] have the potential to be used as active media of semiconductor based metamaterials, yielding negative refraction in the THz spectral range. Perpendicular magnetic field has been added to manipulate the scattering mechanisms and affect the population inversion, which is necessary for achieving high enough degree of population inversion. Comparing these two structures, one can conclude that not all values of magnetic field can provide high values of population inversion. We showed that for both designs, even for the values of magnetic field at which we obtain dips in the gain profile, it is possible to achieve negative values of the real part of ϵ_{\perp} , just by manipulating the total carrier sheet density N_s . Even though those values may be considered very high, they are still manageable. For magnetic field magnitudes between 5.5 and 9.1 T, it is easier to achieve negative refraction with 3-well design, while for other values of B calculations suggest that 4-well structure gives better results. Furthermore, minimum value of the total carrier sheet density needed to achieve negative refraction (negative ϵ_R) is found to be $2 \cdot 10^{16} \text{m}^{-2}$ for both structures, when the applied magnetic fields are greater than 6 T for 3-well design and 7.2 T for the 4-well active region.

Acknowledgements

The authors acknowledge support from MPNS COST ACTION MP1204 - TERA-MIR Radiation: Materials, Generation, Detection and Applications and BMBS COST Action BM1205 - European Network for Skin Cancer Detection using Laser Imaging. This work was also supported by the Ministry of Education, Science and Technological Development (Republic of Serbia), project ev.no. III 45010, and NATO SfP Grant, ref. no. 984068.

References

1. V. G. Veselago, "The electrodynamics of substances with simultaneously negative values of ϵ and μ ", *Sov. Phys. Usp.* **10**, 509-514 (1968).
2. J. B. Pendry, "Negative refraction makes a perfect lens", *Phys. Rev. Lett.* **85**, 3966 (2000).
3. A. N. Grigorenko, A. K. Geim, H. F. Gleeson, Y. Zhang, A. A. Firsov, I. Y. Khrushchev and J. Petrovic, "Nanofabricated media with negative permeability at visible frequencies", *Nature* **438**, 335-338 (2005).
4. A. A. Tavalaae, P. W. C. Hon, Q.-S. Chen, T. Itoh and B. S. Williams, "Active terahertz quantum-cascade composite right/left-handed metamaterial", *Appl. Phys. Lett.* **102**, 021103 (2013).
5. A. A. Tavalaae, P. W. C. Hon, K. Mehta, T. Itoh and B. S. Williams, "Zero-Index Terahertz Quantum-Cascade Metamaterial Lasers", *J. Quan. Elec.* **46**, 1091-1098 (2010).
6. R. A. Shelby, D. R. Smith and S. Schultz, "Experimental verification of a negative index of refraction", *Science* **292**, 77-79 (2001).
7. J. Zhou, Th. Koschny, M. Kafesaki, E. N. Economou, J. B. Pendry and C. M. Soukoulis, "Saturation of the magnetic response of splitting resonators at optical frequencies", *Phys. Rev. Lett.* **95**, 223902 (2005).
8. P. Ginzburg and M. Orenstein, "Nonmetallic left-handed material based on negative-positive anisotropy in low-dimensional quantum structures", *J. Appl. Phys.* **103**, 083105 (2008).
9. L. V. Panina, A. N. Grigorenko and D. P. Makhnovskiy, "Optomagnetic composite medium with conducting nanoelements", *Phys. Rev. B* **66**, 155411 (2002).
10. Z. Liu, P. Hon, A. A. Tavalaae, T. Itoh and B. S. Williams, "Terahertz composite right-left handed transmission-line metamaterial waveguides", *Appl. Phys. Lett.* **100**, 071101 (2012).
11. J. Radovanović, S. Ramović, A. Daničić and V. Milanović, "Negative refraction in semiconductor metamaterials based on quantum cascade laser design for the mid-IR and THz spectral range", *Appl Phys. A* **109**, 763-768 (2012).
12. R. Koehler, A. Tredicucci, F. Beltran, H. E. Beere, E. H. Linfield, A. G. Davis, D. A. Ritchie, R. C. Iotti and F. Rossi, "Terahertz semiconductor-heterostructure laser", *Nature* **417**, 156-159 (2002).
13. A. Benz, C. Deutsch, M. Brandstetter, A. M. Andrews, P. Klang, H. Detz, W. Schrenk, G. Strasser and K. Unterreiner, "Terahertz Active Photonic Crystals for Condensed Gas Sensing," *Sensors* **11**, 6003-6014 (2011).
14. S. Kumar, "Recent Progress in Terahertz Quantum Cascade Lasers", *J. Sel. Top. Quan. Elec.* **17**, 38-47 (2011).
15. A. Daničić, J. Radovanović, D. Indjin and Z. Ikonić, "Modeling of electron relaxation processes and the optical gain in a magnetic field assisted THz quantum cascade laser", *Phys. Scr.* **T149**, 014017 (2012).
16. A. Wacker, "Quantum Cascade Laser: An Emerging Technology", *Nonlinear Laser Dynamics*, Wiley-VCH Berlin (2011).
17. G. Scalari, M. Amanti, C. Walther, R. Terazzi, M. Fisher, M. Beck and J. Faist, "Broadband THz lasing from a photon-phonon quantum cascade laser", *Opt. Express* **18**, 8043-8052 (2010).
18. U. Ekenberg, "Nonparabolicity effects in a quantum well: sublevel shift, parallel mass and Landau levels", *Phys. Rev. B* **40**, 7714-7726 (1989).
19. M. Braun and U. Rossler, "Magneto-optic transitions and non-parabolicity parameters in the conduction band of semiconductors", *J. Phys. C* **18**, 3356 (1985).
20. V. Milanović, J. Radovanović and S. Ramović, "Influence of nonparabolicity on boundary conditions in semiconductor quantum wells", *Phys. Lett. A* **373**, 3071 (2009).

21. P. Basu, "Theory of Optical Processes in Semiconductors: Bulk and Microstructures", Clarendon Press, Oxford (1997).
22. V. A. Podolskiy and E. E. Narimanov, "Strongly anisotropic waveguide as a non-magnetic left-handed system", *Phys. Rev. B* **71**, 201101R (2005).
23. A. Daničić, J. Radovanović, V. Milanović, Z. Ikonić and D. Indjin, "Optimization and magnetic-field tunability of quantum cascade laser for applications in trace gas detection and sensing", *J. Phys. D* **43**, 045101 (2010).
24. G. Scalari, C. Walther, M. Fischer, R. Terazzi, H. Beere, D. Ritchie and J. Faist, "THz and sub-THz quantum cascade lasers", *Las. Phot. Rev.* **3**, 45–66 (2009).
25. S. Kumar, B. S. Williams, Q. Hu and J. Reno, "1.9 THz quantum-cascade lasers with one-well injector", *Appl. Phys. Lett.* **88**, 121123 (2006).
26. C. Jirauschek and T. Kubis, "Modeling techniques for quantum cascade lasers", *Appl. Phys. Rev.* **1**, 011307 (2014).
27. T. Schmielau, M. Pereira, "Nonequilibrium many body theory for quantum transport in terahertz quantum cascade lasers", *Appl. Phys. Lett.* **95**, 231111 (1-3) (2009).
28. T. Schmielau, M. Pereira, "Impact of momentum dependent matrix elements on scattering effects in quantum cascade lasers", *Phys. stat. sol. (b)* **246**, 329-331 (2009).
29. T. Schmielau, M. Pereira, "Momentum dependent matrix elements in quantum cascade lasers", *Microelectronics J.* **40**, 869-871 (2009).
30. A. Wacker, M. Lindskog, D. Winge, "Nonequilibrium Green's functions model for simulation for quantum cascade laser devices under operating condition", *IEEE Journal of Selected Topics in Quantum Electronics* **19**, 1200611 (2013).